analytical chemistry

pubs.acs.org/ac Article

Identification of Hetero-aggregates in Antibody Co-formulations by Multi-dimensional Liquid Chromatography Coupled to Mass Spectrometry

Felix Kuhne, Katrin Heinrich, Martin Winter, Jürgen Fichtl, Gabriel Hoffmann, Franziska Zähringer, Katharina Spitzauer, Monika Meier, Tarik A. Khan, Lea Bonnington, Katharina Wagner, Jan Olaf Stracke, Dietmar Reusch, Harald Wegele, Michael Mormann, and Patrick Bulau*

Cite This: *Anal. Chem.* 2023, 95, 2203−2212 Read Online

ACCESS | Metrics & More | Article Recommendations | Supporting Information

ABSTRACT: Antibody combination therapies have become viable therapeutic treatment options for certain severe diseases such as cancer. The co-formulation production approach is intrinsically associated with more complex drug product variant profiles and creates more challenges for analytical control of drug product quality. In addition to various individual quality attributes, those arising from the interactions between the antibodies also potentially emerge through co-formulation. In this study, we describe the development of a widely applicable multi-dimensional liquid chromatography coupled to tandem mass spectrometry method for antibody homo- versus hetero-aggregate characterization. The co-formulation of trastuzumab and pertuzumab was used, a challenging model system, comprising two monoclonal antibodies with very similar physicochemical properties. The data presented demonstrate the high stability of the co-formulation, where only minor aggregate formation is observed upon product storage and accelerated temperature or light-stress conditions. The results also show that the homo- and hetero-aggregates, formed in low and comparable proportions, are only marginally impacted by the formulation and product storage conditions. No preferential formation of hetero-aggregates, in comparison to the already existing pertuzumab and trastuzumab homo-aggregates, was observed.

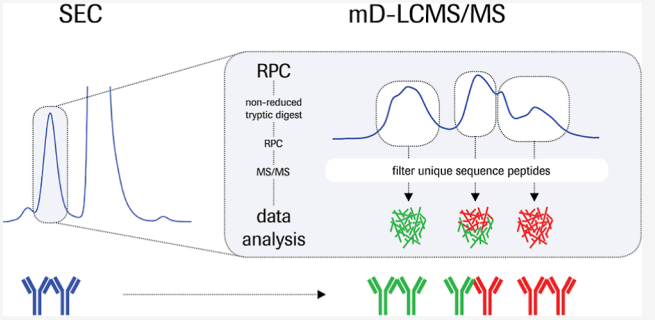

Therapeutic antibodies have become one of the most important therapeutic treatment options for a variety of severe diseases with more than a hundred monoclonal antibody (mAb) products approved by health authorities in the past 35 years.[1,2] To date, various combination therapies are in the development pipelines of the pharmaceutical industry and may improve efficacy without sacrificing patient safety.[3−6] The co-formulation production approach is intrinsically associated with more complex drug product development processes compared to standard mAb products and creates more challenges for manufacturing, process characterization, and analytical control of drug product quality.[7−11] These added challenges are caused by the possible formation of size, charge, and post-translational modification variants due to co-formulation.[12−16] In consequence, product heterogeneities and interactions between the selected components have to be sufficiently characterized prior to final regulatory approval.[17]

Protein aggregates such as mAb dimers and fragmentation products derived from the bioprocess, drug product manufacturing, or storage conditions are critical product-related impurities for mAb formats. These size variants require extensive characterization and close monitoring as they can cause immunogenic responses, or they may exhibit different pharmacokinetics or potency compared to the desired product.[18,19] In recent years, highly concentrated drug product formulations for subcutaneous administration have gained in importance, with high concentrations inherently also increasing the risk of aggregation. Moreover, many of the new emerging mAb formats exhibit increased structural complexity and hence the potential heterogeneity of the degradation products is also increased. For the routine analysis of product size variants, size-exclusion high-performance liquid chromatography (SE-HPLC) combined with UV detection is generally applied for quality control testing of biologics.[20] Limitations of SE-HPLC are the relatively low resolution for the separation of high-molecular weight (HMW) aggregates and that it does not allow accurate mass determination of the detected species within the analyzed protein sample. Alternatively, application

Received: July 18, 2022
Accepted: January 10, 2023
Published: January 20, 2023

https://doi.org/10.1021/acs.analchem.2c03099
Anal. Chem. 2023, 95, 2203−2212

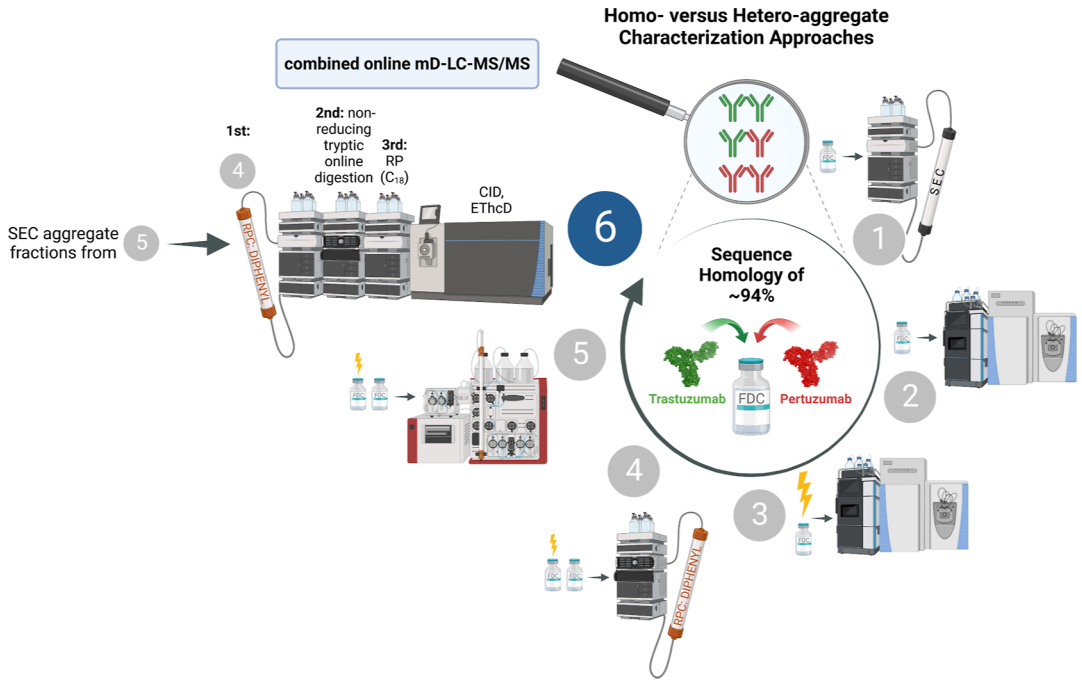

Figure 1. Homo- vs hetero-aggregate characterization approaches. (1) SE-HPLC, (2) size-exclusion chromatography coupled to MS (SEC-MS), (3) forced degradation approach (light-stress) and subsequent SEC-MS analysis, (4) RP-UHPLC, (5) preparative SEC sample fractionation, and (6) combined online mD-LC−MS/MS approach. Created with BioRender.com.

of multi-angle light scattering detection with moderate mass accuracy or high-resolution mass spectrometry (MS) is commonly utilized to overcome these limitations, both for the analysis of antibody monomers and for complexes thereof.[21−25]

During recent years, several authors have successfully demonstrated the application of two- or multi-dimensional LC coupled to MS (2D- or mD-LC−MS) methods for the qualitative and quantitative structural characterization of therapeutic antibodies and related protein formats.[26−31] The mD-LC−MS approach combines sample preparation and multi-level analysis of antibody attributes within an automated continuously connected setup (online) and removes the need for manual sample preparation procedures and sample handling (offline).[32,33]

In this study, we describe the development of a widely applicable, mD-LC−MS/MS method for antibody aggregate characterization, using the co-formulation or fixed-dose combination (FDC) of pertuzumab and trastuzumab, recently approved as Phesgo, as the model analyte (for an overview of the experimental design, see Figure 1). An approach employing light-stress conditions and various separation techniques combined with mD-LC−MS/MS facilitated detailed assessment of the highly similar and hence difficult to distinguish dimer variants. This test system enabled discrimination between homo- versus hetero-aggregation and provides an effective methodology for size variant evaluation in recombinant antibody co-formulations.

MATERIALS AND METHODS

Samples. All samples used in this study were engineered, manufactured, and purified in-house. Individual formulations of trastuzumab and pertuzumab and the FDC co-formulation of trastuzumab/pertuzumab (1:1 mass ratio) were used. Samples were generally formulated at 120 mg/mL in 20 mM histidine/histidine-HCl, 105 mM trehalose, 100 mM sucrose, 10 mM methionine, and 0.04% [w/v] polysorbate 20 (Tween) buffer at pH 5.5 (using diluted HCl or NaOH), herein referred to as the formulation buffer. In a subset, this reference material (RM) was light-stressed, that is, light-exposed at 250 Wh/m^2 for 72 h in a SUNTEST XLS+ lightfastness test chamber (AMETEK), to obtain light-stress material (LSM). The test chamber was cooled to ensure temperatures between 20 and 28 °C. All samples were stored at −20 °C.

Size Variant Analysis (SE-HPLC). The separation of size variants was performed with an UltiMate 3000 HPLC system (Thermo Fisher Scientific) using a TSKgel G3000SWXL size-exclusion chromatograph column (Tosoh Bioscience, cat no. 08541, 5 μm, 7.8 × 300 mm). Data were recorded by UV detection at 280 nm (UV_{280}), and data analysis was done using the Chromeleon chromatography data system (CDS) software (Thermo Fisher Scientific). The mobile phase buffer composed of 0.2 M potassium phosphate and 0.25 M KCl at pH 6.2 was used. A molecular weight standard demonstrated the system suitability. Prior to loading, the samples were diluted to 30 mg/mL with formulation buffer, and 5 μL (150 μg) of sample was injected per run. The following analytical conditions were applied: 0.5 mL/min flow rate, 25 ± 2 °C column temperature, 5 ± 4 °C auto-sampler temperature, and 30 min under isocratic conditions. Relative areas under the curve (AUCs) were used to calculate the percentage areas from the total area of all peaks observed.

Size Variant Identification (Native Size Exclusion Chromatography−MS). Size variants were identified as previously described.[34] In brief, the separation was accomplished with an ACQUITY BEH size exclusion chromatograph column (Waters, cat no. 186005226, 1.7 μm, 4.6 × 300 mm) installed on a Vanquish Flex ultra-high performance liquid chromatography (UHPLC) system (Thermo Fisher Scientific) with detection at UV_{280}. The UHPLC system was coupled to a

https://doi.org/10.1021/acs.analchem.2c03099
Anal. Chem. 2023, 95, 2203−2212

Q Exactive ultra-high mass range mass spectrometer equipped with an in-house extended Nanospray Flex ion source (Thermo Fisher Scientific). UHPLC data acquisition and processing were performed using Chromeleon CDS (Thermo Fisher Scientific). MS data were recorded with Xcalibur software (Thermo Fisher Scientific). Before injection, the samples were diluted to 1 mg/mL in 20 mM His−HCl buffer at pH 6. Per injection, approximately 20 μg sample was loaded onto the column. The following UHPLC measurement conditions were applied: 0.25 mL/min flow rate, 25 ± 2 °C column temperature, 5 ± 2 °C auto-sampler temperature, and 30 min under isocratic conditions with 100 mM ammonium acetate buffer. For MS, ion in-source trapping at −175 V and in-source collision-induced dissociation with 30 eV were applied. After trapping in the C-trap, ions were detected at a resolution of 12,500 at m/z 400 (R_{set}). MS data were analyzed using Byos software (Protein Metrics). The intact mass module allowed the mass deconvolution and assignment.

Analysis of Chemical Modifications (LC−MS/MS Tryptic Peptide Mapping). The protein samples were first denatured by diluting to a concentration of 1 mg/mL with a buffer solution containing 6 M guanidinium chloride, 300 mM tris(hydroxymethyl)aminomethane (Tris), and 2 mM ethylenediaminetetraacetic acid at pH 7.0. This was followed by reduction, accomplished by adding 4 μL of 1 M 1,4-dithiothreitol (DTT) solution to each 250 μg (in 250 μL) sample and incubating at 37 °C for 60 min. After short cooling, the free thiols were carboxymethylated by the addition of 10.4 μL of 1 M iodoacetic acid solution per sample and 15 min incubation at room temperature in the dark. The alkylation reaction was stopped with 2 μL of 1 M DTT solution per sample. Samples were then buffer-exchanged with 50 mM Tris−HCl, 2 mM $CaCl_2$, pH 7.5 digestion buffer using NAP Sephadex desalting columns (Cytiva, cat no. 17-0853-02). Protein digestion was accomplished by 1:20 [E/S] dilution with 0.2 μg/μL trypsin solution (Roche, cat no. 03708985001) and subsequent incubation at 37 °C for 60 min. The reaction was stopped with 5 μL of 54 mM methionine in 80% trifluoracetic acid (TFA).

Sample digests were then separated on an ACQUITY ultra-performance liquid chromatography (UPLC) system (Waters) equipped with an analytical ACQUITY CSH C_{18} reversed-phase (RP) column (Waters, cat no. 186006938, 1.7 μm, 2.1 × 150 mm) and detected online with an Orbitrap Fusion mass spectrometer (Thermo Fisher Scientific). UPLC data were acquired and analyzed with Chromeleon CDS (Thermo Fisher Scientific). Mass spectra were recorded with Xcalibur software (Thermo Fisher Scientific). The mobile phases were composed of 0.1% [v/v] formic acid (FA) in purified water (mobile phase A) and acetonitrile (ACN, mobile phase B). The following UPLC system settings were applied: 0.3 mL/min flow rate, 65 ± 2 °C column temperature, 10 ± 2 °C auto-sampler temperature, 90 min linear gradient from 1 to 35% mobile phase B, followed by 5 min ramping-up to 65% mobile phase B and two times 3 min cleaning at 80% mobile phase B. Approximately 3−6 μg sample was injected per analysis. Protein absorbance was monitored by UV_{220}. Relevant system suitability tests and control samples were included in the analytical sequences. MS1 precursor detection was enabled at an R_{set} of 60,000 (Orbitrap). MS2 fragment ions were generated with 35% collision-induced dissociation (CID) energy and 10 ms activation. Data-dependent acquisition was automatically sorted by prioritized fragmentation of most intense precursors.

Recorded data were analyzed with Byos (Protein Metrics). Relevant peptides were verified on the MS2 level. Based on their extracted ion chromatogram (XIC) areas, relative abundances of modified peptides were calculated as the percentage over all corresponding wild- and modified-type peptides.

Note: FDC HMW1 size variant fraction and corresponding RM (Table S3) were measured and analyzed as previously described.[35,36]

Isolation of Size Variants (Preparative SEC). Size variants from the RM and LSM were fractionated by use of an ÄKTA avant 25 chromatography system (Cytiva) equipped with a Superloop assembly for automated sample injection and a built-in fraction collector with cooling function. The separation was achieved using a HiLoad 26/600 Superdex 200 pg preparative size exclusion chromatograph column (GE Healthcare, cat no. 28989336) and the UNICORN software (GE Healthcare) for system control. The system was operated at 2.6 mL/min flow rate and 0.5 mL/min while injecting. The mobile phase was 20 mM histidine/histidine-HCl, 105 mM trehalose, 100 mM sucrose, 10 mM methionine, and 150 mM NaCl buffer at pH 5.5. The column was operated at ambient temperature and protein absorbance was monitored by UV_{280}. The isolation of size variants was accomplished by fraction collection over multiple repeat cycles. The collected fractions were analyzed by analytical SE-HPLC and pooled accordingly to generate pure size variant samples. Size variant pools were buffer-exchanged (with Tween-free formulation buffer) and concentrated using a Sartoflow Smart crossflow system (Sartorius) equipped with Pellicon 3 Cassette and Biomax membranes (Millipore, cat no. P3B030A01, 30 kDa, 0.11 m^2), or Amicon stirred cells (Millipore). Concentrations were determined using a NanoDrop 2000c (Witec).

Separation of Co-formulated mAbs (RP-UHPLC). Separation of polarity variants by reversed-phase chromatography (RPC) under denaturing conditions was conducted on an UltiMate 3000 RS UHPLC system (Thermo Fisher Scientific) using an analytical ZORBAX RRHD diphenyl RP-column (Agilent Technologies, cat no. 858750-944, 1.8 μm, 2.1 × 100 mm). Instruments operating on Empower (Waters) and Chromeleon CDS (Thermo Fisher Scientific) software platforms were used for instrument control and data acquisition. Mobile phase A composed of 98:2 [v/v] H_2O/2-propanol and 0.1% [v/v] TFA and mobile phase B composed of 70:20:10 [v/v/v] 2-propanol/ACN/mobile phase A were used. The following run conditions were applied: 0.3 mL/min flow rate, 70 ± 2 °C column temperature, 10 ± 4 °C auto-sampler temperature, 15 min linear gradient from 30 to 45% mobile phase B and 5 min cleaning with 90% mobile phase B. Samples were diluted to 1 mg/mL with the formulation buffer. Approximately 100 μg sample was injected per run. Protein absorbance was monitored by UV_{280}.

Dimer Analysis by Non-reducing mD-LC−MS/MS. An in-house extended 1290 Infinity II 2D-LC system (Agilent Technologies) comprising the following modules was used for online mD-LC analyses: a 1260 Infinity II bio-inert pump (first dimension), a 1290 Infinity II flexible pump coupled to a 1260 Infinity capillary pump (second dimension), and a 1290 Infinity high-speed pump (third dimension). System control, data acquisition, and data analysis were performed with OpenLab CDS ChemStation (Agilent Technologies).

https://doi.org/10.1021/acs.analchem.2c03099
Anal. Chem. 2023, 95, 2203−2212

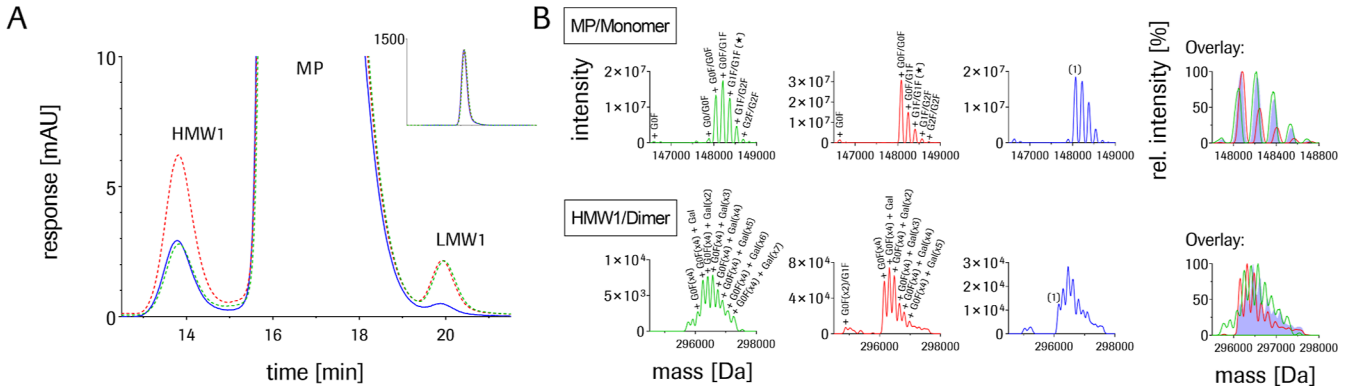

Figure 2. Size variants of trastuzumab (green), pertuzumab (red), and FDC (blue) RM. (A) Size variants separated by SE-HPLC. Peak annotation: high-molecular weight 1 (HMW1) species, main peak (MP), and low-molecular weight 1 (LMW1) species. Inset shows the full signal scale. Associated relative areas (AUC) of the chromatographic peaks are presented in Table S1. (B) Size variant identification by native SEC-MS, indicated on the deconvoluted mass spectra (calculated and observed mass values are given in Table S2 for selected species). Top panels show the antibody monomers identified in the MP peak. Bottom panels show the antibody dimer species identified in the HMW1 peak. (*) indicates "or G0F/G2F." (1) Reference mass assignment shown in Table S2. Mass accuracy for proteoform assignment: <10 Da for monomers and <30 Da for dimers.

Samples were first diluted to 1 mg/mL with the formulation buffer. Aliquots were injected on the first dimension and separated by RPC, as described in the previous section. The separated variants were isolated as online fractions, henceforth described as cuts, and collected in sample loops (120 μL capacity). The subsequent sequential transfer of the cuts to the second dimension was software-automated and pre-programed. The transfer, executed in the reverse order of loop storage, was achieved by the employment of an active solvent modulation valve. A dilution of 5:1 of the samples was used to address the solvent compatibility issues between the first and second dimensions. In the second dimension, tryptic protein digestion was accomplished with a customized trypsin column (Thermo Fisher Scientific, immobilized trypsin, TPCK-treated agarose resin, cat no. 20230, column packed by Dr. Maisch GmbH, 2.1 × 100 mm) under non-reducing conditions. As mobile phase, 50 mM Tris and 10 mM $CaCl_2$ buffer at pH 8.0 was utilized. Isocratic conditions with 0.25 mL/min flow rate and 26 min digestion time at 50 ± 1 °C column temperature were applied. Eluting peptides were intermediately trapped on an ACQUITY UPLC BEH C_{18} VanGuard pre-column (Waters, cat no. 186003975, 1.7 μm, 2.1 × 5 mm). Third dimension: peptide separation was achieved with an ACQUITY BEH C_{18} RP column (Waters, cat no. 186002353, 1.7 μm, 2.1 × 150 mm) and performed as described in the previous section. The separated peptides were detected online with an Orbitrap Fusion mass spectrometer (Thermo Fisher Scientific), likewise described in the previous section. In addition to CID, electron-transfer/higher-energy collisional dissociation (EThcD) for large precursor fragmentation was used. Supplemental activation was applied with 30% collision energy subsequent to 50 ms ETD reaction time (reagent target of 5.0×10^5).

Recorded data were analyzed with Byos (Protein Metrics) and self-written R scripts (RStudio). Unique sequence peptides among trastuzumab and pertuzumab were verified on MS2 level with Byos. Lists of identified peptides were imported to RStudio for further data processing. For comparison of the first dimension cuts, the relative change in the unique sequence peptide XIC areas was determined by normalization of equally charged unique sequence peptide subsets on highly abundant reference peptides with trastuzumab/pertuzumab-shared sequences (n = 3), resulting in normalization subsets. Subset means and standard deviation were compared for unique sequence segments among trastuzumab and pertuzumab (shown in Figures 3B and 4B).

RESULTS AND DISCUSSION

Characterization of Trastuzumab/Pertuzumab Single- and Co-formulation(s). Co-formulated antibodies are usually compared to the corresponding individual formulations for analytical characterization and evaluation. The quality attributes of the co-formulation should directly correspond to those of the individual mAbs. Due to a high sequence homology of 93.5%, trastuzumab and pertuzumab are highly similar in their physicochemical properties and molecular weight. The analytical separation to characterize their HMW size variants is therefore challenging.

The first characterization step involved analyzing individually the size variants of identically formulated RM of the single- and co-formulation(s). First, the size variants were separated by SE-HPLC, and using UV_{280} detection 0.3% (trastuzumab), 0.6% (pertuzumab), and 0.3% (FDC) relative amounts were obtained for the HMW1 species (Figure 2A and Table S1). Also, importantly, no additional HMW variants were detected by SEC and UV detection (SEC-UV) for the FDC.

Native SEC-MS analysis identified the MPs as heterogeneously Fc-glycosylated antibody monomers with mass values between 148 and 149 kDa. The HMW1 variants were identified as likewise heterogeneously Fc-glycosylated antibody dimers with mass values between 296 and 297 kDa. Figure 2B shows the deconvolution mass spectra of the Fc glycoform distributions of the antibody monomers (top panels) and antibody dimers (bottom panels) for the individually formulated mAbs and their co-formulation. Table S2 gives an example of selected theoretical and experimentally determined mass values. For the individually formulated mAbs, mass values could be determined with a mass accuracy of <10 Da for monomers and <30 Da for dimers. The two single molecules also differ in their Fc glycosylation distributions. Assignments for the major glycoforms for the monomers and dimers of trastuzumab and pertuzumab are provided as annotations in the spectra (cf. Figure 2B). However, the complex mass spectra of the monomers and dimers in the co-formulation did not

https://doi.org/10.1021/acs.analchem.2c03099
Anal. Chem. 2023, 95, 2203−2212

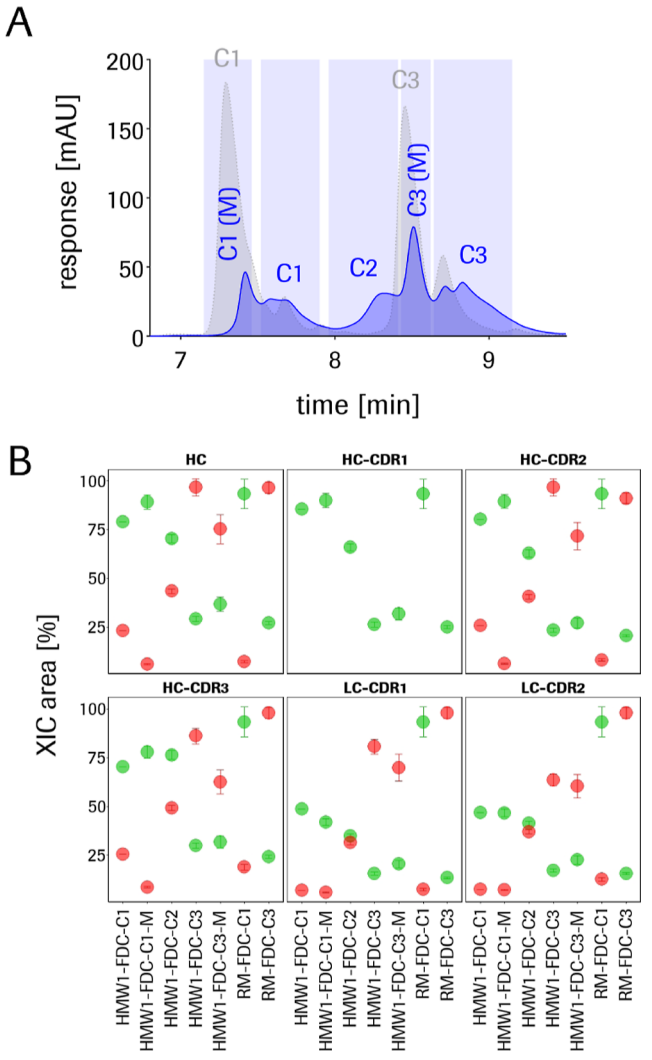

Figure 3. mD-LC−MS/MS separation and identification of FDC trastuzumab/pertuzumab homo- and hetero-aggregation. Non-stressed RM FDC HMW1 size variant fraction (see Figure S4A), analyzed by mD-LC−MS/MS. Tested samples are termed as follows: [size variant pool or starting material]-[formulation or mAb]-[first dimension cut], for example, HMW1-FDC-C1. (A) mD-LC first dimension RP-UHPLC chromatograms of RM FDC (gray, dotted line) and RM FDC HMW1 pool (blue, solid line). RM FDC HMW1 first dimension cuts and subsequent material transfer to the mD-LC second dimension are indicated by blue transfer windows and annotated with "C1" to "C3." Additional "M" indicates simultaneous elution with MP/monomer variants. (B) Relative XIC area (mean and standard deviation of normalization subsets, n = 3) of trastuzumab (green dots) and pertuzumab (red dots) equally charged (z = 2) unique sequence peptides of FDC samples from (A) determined by mD-LC−MS/MS. Unique sequence segments: heavy chain (HC) or light chain (LC) complementarity-determining regions (CDR) 1−3.

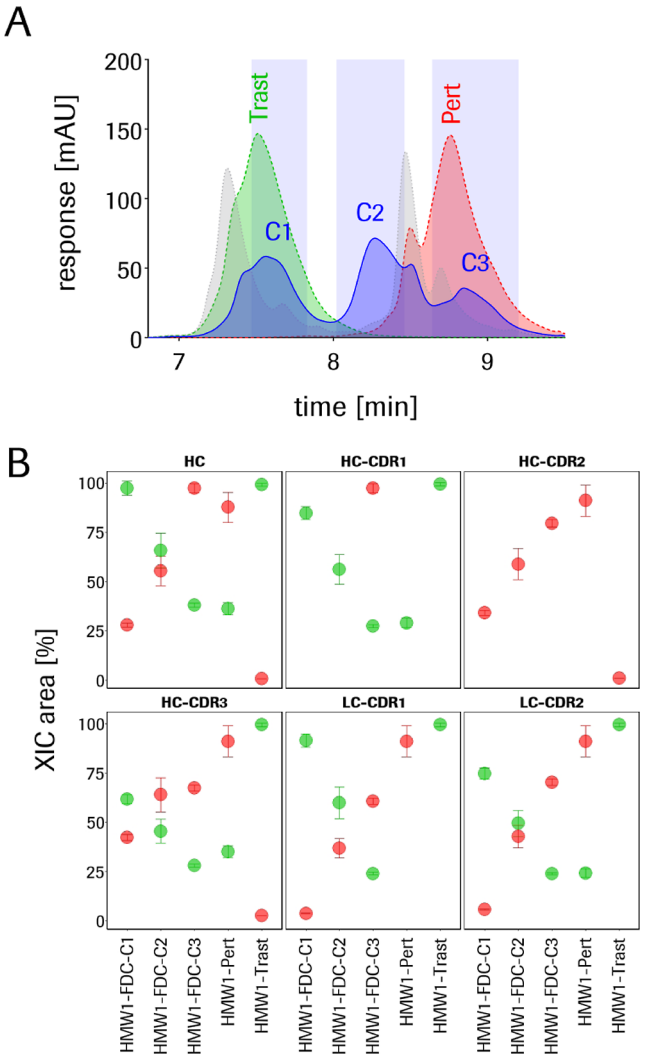

Figure 4. mD-LC−MS/MS separation and identification of FDC LSM homo- and hetero-aggregation. LSM FDC and single product formulation (trastuzumab, pertuzumab) HMW1 size variant fractions (see Figure S4C), analyzed by mD-LC−MS/MS. (A) mD-LC first dimension RP-UHPLC chromatograms of LSM: FDC (gray, dotted line) and trastuzumab (Trast: green, dashed line), pertuzumab (Pert: red, dashed line), and FDC (blue, solid line) HMW1 pools. LSM FDC HMW1 first dimension cuts and subsequent material transfer to the mD-LC second dimension are indicated by blue transfer windows and annotated with "C1" to "C3." (B) Relative XIC areas (mean and standard deviation of normalization subsets, n = 3) of trastuzumab (green dots) and pertuzumab (red dots) equally charged (z = 2) unique sequence peptides of LSM samples from (B) determined by mD-LC−MS/MS.

resolve the individual antibodies or antibody dimer variants. We could only obtain a single, "average" proteoform distribution for the FDC monomer (~30 Da delta mass), and dimer species (~60 Da delta mass), also shown in an overlay together with the individual molecules in Figure 2B. A distinction between the different dimer species in the co-formulation was not possible.

The low abundance of HMW1 species for single and co-formulation RM posed an additional analytical challenge for aggregate characterization. Stability studies over 36 months at 5 °C and accelerated stability studies for 12 months at 25 °C confirmed only minor changes in the FDC size variant content (Figure S1). As assessed by SEC-UV, we could observe that MP areas decreased by only ~0.4% (Figure S1 A, right panel) and HMW1 areas increased by only ~0.2% after 36 months at 5 °C (Figure S1B, right panel). Minor conversion to HMW1 species (~0.4%) was also observed at elevated temperature conditions (25 °C) after 12 months (Figure S1B, left panel). The stability data confirm that pertuzumab and trastuzumab are not prone to aggregation and that no significant formation of HMW variants occurs during manufacturing or storage of the FDC drug product.

https://doi.org/10.1021/acs.analchem.2c03099
Anal. Chem. 2023, 95, 2203−2212

While the stability of the FDC leads to a challenging model system for developing strategies to investigate HMW formation in co-formulations, through this, we could identify methods enabling conclusive and unambiguous differentiation and identification of highly analogous species.

Light-Stress-Induced Antibody Dimerization. As already reported in previous studies, light initiates and accelerates the aggregation of antibodies.[37−39] Intermolecular interactions can form via various photodegradation pathways.[40,41] We used harsh light-stress conditions to induce the formation of intermolecular interactions between the co-formulated antibodies. With this, we increased the aggregate content to enable the establishment of an analytical test system for the identification of homo- and hetero-aggregate formation.

Figure S2 shows results from the single- and co-formulation(s) after 72 h of light-stress at 250 Wh/m^2. An increase in the HMW1 content up to 6.1% (trastuzumab), 9.0% (pertuzumab), and 8.5% (FDC) was determined by SEC-UV analysis (Figure S2A, Table S1). Additionally, up to 1% HMW2 species were induced by the light-stress conditions in pertuzumab. This species could be assigned as the trimer using SEC-MS (full results given in Table S1). For all LSM samples, predominantly increased dimer (HMW1) levels were determined. Nevertheless, a differentiation of the co-eluting dimer variants was not achievable by SEC-UV alone. Peptide mapping analysis revealed that light-stress mainly resulted in significant increases in methionine oxidation levels (Figure S2B, Table S3) for all formulations. Methionine oxidation at the conserved Fc amino acid 25× (EU numbering) was raised to 49, 54, and 57% (from 3, 4, and 4% for trastuzumab, pertuzumab, and FDC, respectively).[42] Comparable trends were observed for the Fc methionine at position 43×.

Remarkably, even after such harsh light-stress conditions resulting in extremely high oxidation values, and therefore presumably advanced photo-degradation, only a moderate increase in the HMW content, mainly dimers, could be determined. Pertuzumab was found to be slightly more prone to dimerization compared to trastuzumab. However, as already observed for the non-stressed RM, no further differentiation of the potential homo- or hetero-aggregate species was achievable for the enriched dimer (HMW1) peak by SEC-MS (data not shown).

Separation of Co-formulated mAbs by RP-UHPLC. Trastuzumab and pertuzumab differ primarily in their CDRs. Pertuzumab LC CDRs are composed of several hydrophobic isoleucine (and tyrosine) residues. Trastuzumab is therefore slightly more hydrophilic and elutes earlier in RPC, enabling chromatographic separation of the two products.

We used this characteristic and developed a RP-UHPLC method, utilizing a diphenyl-bonded stationary phase, to separate co-formulated trastuzumab from pertuzumab. Hereby, FDC RM was separated in two peak "clusters," each comprising a MP and followed by smaller partially but not base-line resolved peaks (Figure S3A). RP-UHPLC of individual single product formulations revealed the clear separation of the molecules trastuzumab and pertuzumab, which also allowed the assignment of the molecules in the FDC. A comparable separation profile was observed for LSM samples but with broader peaks and slightly more tailing (Figure S3B). Despite the increased dimer content and significantly raised oxidation levels for the LSM samples, no new peaks could be distinguished visually.

Isolation and Analysis of Co-formulation Dimer Variants. In order to differentiate and identify HMW variants potentially separated by the RP-UHPLC, we isolated the HMW1 fractions of RM and LSM by preparative SEC followed by peak fractionation.

From the non-stressed RM, a HMW1 fraction with ∼80% dimer purity could be isolated (Figure S4A). Relevant amino acid degradations were found unchanged compared to the corresponding starting material [Table S3, column "HMW1 (Pool)"]. Native SEC-MS measurements of the enriched HMW1 dimer fraction of the co-formulated FDC, however, still yielded overlapping signals and hence inconclusive results (Figure S4B).

This was also observed for the dimer fraction of the light-stressed FDC material. The enriched HMW1 fraction of the LSM yielded ∼90% dimer purity for single and co-formulated materials (Figure S4C) as demonstrated by analytical SEC-UV testing. LC−MS/MS peptide mapping data confirmed no experimental artifacts caused by the fractionation and subsequent sample preparation. Modification abundances were comparable for all LSM versus LSM HMW1 samples (Table S3). However, as already mentioned, light-stress leads to various structural and chemical modifications and therefore to an increase in heterogeneity, that is, a larger number of proteoforms. Using native SEC-MS, we observed accumulated mass increases (between 50 and 95 Da) for the dimer fractions. In Figure S4D the corresponding RM distributions are plotted for comparison (in gray). A more narrow and shifted proteoform distribution can be observed for the LSM dimer samples of trastuzumab (in green) and pertuzumab (in red) as compared to the non-stressed material.

Higher chromatographic or mass spectrometric resolution of the dimer variants could not be achieved despite the highly resolving techniques applied. Hence, with the goal of further characterizing the FDC RM and FDC LSM dimer material, the isolated and enriched HMW1 variants were further analyzed using RPC-UV.

Separation of SEC-Isolated Dimer Variants by RP-UHPLC. In Figures 3A and 4A, numbered segments or windows dividing the (first dimension) RPC-UV chromatograms are shown. The chromatographic profiles obtained were comparable to those obtained with the offline method shown in Figure S3. The material contained in each window, called cuts, was subsequently transferred separately, online, to further LC dimensions as described in the next section.

The isolated dimer fraction derived from RM showed a different peak distribution in the RPC-UV chromatogram compared to the corresponding starting sample (Figure 3A, HMW1 curves in blue and RM in gray, respectively). Thus, the separation based on differences in the hydrophobicity enabled an additional separation of the SEC-isolated HMW1 fractions. In contrast to the RM sample, also shown in Figure S3A, we observed the main peak (M) at lower intensity and the peaks putatively corresponding to the HMW1 variants at higher abundances (C1, C2, and C3).

For the HMW1 variants fractionated from LSM, the peaks C1−C3 were observed with even higher abundance but less resolved compared to the RM HMW1 (Figure 4A). This phenomenon is most likely a result of the increased heterogeneity induced by the raised structural modification levels from light-stress, especially oxidation (results are summarized in Table S3). In addition, compared to LSM co-formulation, the peak shapes of LSM trastuzumab dimer pool

https://doi.org/10.1021/acs.analchem.2c03099
Anal. Chem. 2023, 95, 2203−2212

and LSM pertuzumab dimer pool (Trast and Pert in Figure 4A) were relatively similar. The trastuzumab dimer elutes with the same retention time of the FDC HMW1 C1 peak and likewise the pertuzumab dimer with the FDC HMW1 C3 peak. The RPC peaks C1 and C3 of the FDC dimer fraction could therefore be clearly assigned to the homodimers of trastuzumab and pertuzumab, respectively.

Interestingly, we observed an additional peak (C2) for both isolated FDC HMW1 fractions (RM and LSM) that was not detected in the dimer fractions of the individual formulations. This observation suggests the presence of trastuzumab/pertuzumab hetero-aggregates, at a corresponding intermediate hydrophobicity (Figures 3A and 4A).

As indicated by the higher intensities of the C1, C2, and C3 peaks for the LSM HMW1 fraction, it is also likely that further covalent interactions are induced by the harsh light-stress conditions. The results of the HMW1 from the non-stressed material (RM), however, indicate that the aggregation may be partially due to non-covalent interactions. Higher abundances for the main peak (M, Figure 3A), corresponding to the dissociated monomers can be observed under these non-native LC conditions. Nevertheless, at this point, we had already succeeded in separating at least three different variants from the HMW1 fraction of the co-formulation using diphenyl-RPC. Further analytical characterization of the intermediate polarity C2 peak was addressed by mD-LC−MS/MS.

Separation of Isolated Dimer Variants and Identification of Hetero-aggregates by mD-LC−MS/MS. An online mD-LC−MS/MS solution comprising RP-UHPLC followed by peptide mapping was developed to improve the isolation and identification of the aggregate variants. Since we had already isolated fractions of the size variants of interest, and separation of prominent HMW variants (C1−C3) could be accomplished by means of RPC, a combined mD-LC−MS/MS setup for the separation, identification, quantification, and characterization of the HMW variants was the logical next step. Figure S5 shows a schematic representation of the mD-LC−MS/MS configuration. The previously developed RP-UHPLC was applied in the first dimension, and we applied a non-reduced tryptic online digestion for the second dimension. In this way, aggregates derived from disulfide interactions could also be identified, if present. The tryptic peptides obtained were separated in the third dimension using a C_{18} RPC column. This mD-LC system was coupled to a high-resolution Orbitrap Fusion mass spectrometer for the identification and semi-quantitative determination of the peptides. Peptide identification was accomplished via CID and EThcD gas phase fragmentation and MS2 fragment ion identification. The description and relative quantification of only the molecule-specific sequence peptides, that is, peptides from unique sequence segments of the single molecules trastuzumab or pertuzumab, are included here. These are referred to as unique sequence peptides in the following sections.

The corresponding unique antibody sequence segments, namely HC, HC CDR1-3, and LC CDR1-2, are presented in sub-panels in Figures 3B and 4B, and referred to as sequence segment panels in the following text. Furthermore, disulfide-bridged peptides within unique sequence segments are shown in Figure S6A,B, namely peptides linked by cysteine 22 and 96 (22C $ C96) as well as peptides linked by cysteine 23 and 88 (23C $ C88).[42] The analyzed cuts in Figures 3 and 4 are termed as follows: [size variant pool or starting material]-[formulation or mAb]-[first dimension cut], for example, HMW1-FDC-C1. For all cuts, the relative abundances of trastuzumab (in green)- and pertuzumab (in red)-specific peptides, that is, unique sequence peptides, are shown. The XIC areas thus represent material collected in the first dimension (RPC). Peaks were isolated and transferred according to predefined cut times (blue windows in Figures 3A and 4A) and labeled C1−C3 as previously introduced. Furthermore, for comparative purposes, the non-stressed RM and LSM HMW1 fractions of the single molecule formulations were analyzed and quantified analogously.

Overall, by mD-LC−MS/MS, we determined that the unique sequence peptides were present with varying relative XIC areas between the RPC-separated dimer variants. In Figures 3B and 4B the relative quantification of the peptide abundances reveals a repeating pattern of mAb-specific peptide abundances that can be observed among RM (Figure 3B) and LSM (Figure 4B) for all of the unique sequence segment panels.

For example, in the top left panel of Figure 3B, pertuzumab unique peptides (in red) were determined to be present in low abundance for the C1 peak of the non-stressed co-formulated dimer pool (HMW1-FDC-C1 and HMW1-FDC-C1-M). For unique pertuzumab sequence peptides, relative abundances then increase for peaks C2 and C3, respectively. The opposite trend was observed for unique trastuzumab sequence peptides. The non-fractionated (SEC) RM starting sample was included here as a control sample. As expected, the RPC-separated RM peaks C1 and C3 (Figure 3A in gray and Figure S3A in blue) showed high trastuzumab peptide abundance values for the C1 and high pertuzumab values for the C3 peak and the inverse, that is, low trastuzumab values for the C3 and low pertuzumab values for the C1 peak. The trastuzumab unique sequence peptide intensities from the C2 peak, which could only be detected in the co-formulated HMW1 material, were consistently lower than the intensities of the corresponding C1 peak and higher than the intensities of the corresponding C3 peak. The trends for pertuzumab-specific peptides were found to be the inverse. In comparison to the C2 peak, lower intensities for the C1 peak and higher intensities for the C3 peak were determined. These trends were even more pronounced for LSM samples (Figure 4B). The isolated HMW1 variants of the individually formulated mAbs were used as controls for the LSM runs. Consequently, the C2 peaks could be assigned as a mixture of trastuzumab and pertuzumab peptides with similar intensities, corresponding to a hetero-aggregate parent molecule.

Comparable trends were also determined for disulfide-linked peptides within unique trastuzumab or pertuzumab sequence segments (Figure S6A,B). Compared to the observed abundances for the other unique sequence peptides, no obvious changes in the disulfide-bridged peptides of homo- and hetero-aggregate dimer or between non-stressed and stressed dimers were found, for example, structural changes due to potential light-stress-induced disulfide shuffling could not be detected. Neither such intermolecular shuffled peptides could be detected in the recorded peptide mapping data sets. According to the data, the hetero-aggregation is therefore not elicited by shuffled disulfide bridges, at least not by the disulfide bridges of the unique sequence segments described here.

Overall, the recurring trend pattern across different sequence segments confirms the validity of the results. The composition of the RPC-separated HMW1/dimer variants can be derived

https://doi.org/10.1021/acs.analchem.2c03099
Anal. Chem. 2023, 95, 2203−2212

very clearly from the results. The relative peptide intensities determined three different dimer variants in co-formulated trastuzumab/pertuzumab FDC for both reference and light-stress dimer materials. The obtained data verified the C1 peak as trastuzumab homo-dimer, the C2 peak as trastuzumab/pertuzumab hetero-dimer, and the C3 peak as pertuzumab homo-dimer.

CONCLUSIONS

The present study demonstrates the challenges in distinguishing and characterizing similar HMW size variants in antibody co-formulations. The trastuzumab/pertuzumab co-formulation aggregate assessment represents a most demanding example, adding value to other recent studies with less related co-formulated antibody products.[7,43] The presented data verify the high stability of the trastuzumab/pertuzumab co-formulation where only minor aggregate formation is observed with product storage and accelerated temperature conditions (below 1%).

Even with harsh light-stress conditions, less than 10% dimer content was observed. Furthermore, the interaction between trastuzumab and pertuzumab has not been previously reported. In this study, we were able to show that for the trastuzumab/pertuzumab co-formulation, the proportion of heterogeneous interactions corresponds to the individual proportions of homogeneous interactions. The results also suggest that the low-abundant formation of trastuzumab/pertuzumab homo-aggregates and similar amount of hetero-aggregates at RM level occur mainly during bioprocessing, and product storage conditions have a limited impact. Comparable homo- versus hetero-aggregate formation was also observed after applying harsh light-stress conditions. The observations do not suggest the preferential formation of pertuzumab/trastuzumab hetero-aggregates in addition to the already existing pertuzumab and trastuzumab homo-aggregates; however, a conversion between homo- and hetero-aggregates at the minimal level cannot be excluded.

Native SEC-UV and SEC-MS were not capable of differentiating the small mass difference between the pertuzumab and trastuzumab dimer species at intact antibody level. Due to the lower resolution settings, such as the one chosen, the mass accuracy/precision for individually formulated monomers was ∼27 ppm for the selected glycoforms (see Table S2). We are currently improving our online SEC-MS system to achieve better resolution/mass accuracy by testing different instrumental settings such as chromatographic and desolvation conditions. However, the identification and differentiation between homo- and hetero-aggregates was only feasible using pre-enriched dimer fractions in combination with multidimensional LC and MS detection. The mD-LC−MS/MS approach adopted here not only allowed the online separation of dimer variants but also enabled, in combination with accurate mass determination, the identification of product-specific peptides and subsequent relative quantification. The characterization of various degradation (including fragments, oxidative, and other chemical degradation products) and low-abundant product variants such as sequence variants, non-consensus glycosylation, and glycation can also be achieved, delivering information covering a wide range of attributes in one method. The non-reducing mD-LC−MS/MS method also enabled the detection of disulfide bridges. However, despite using various samples and applying orthogonal methods, how the different dimer variants interact with each other could not be deduced. Even after exposure to light, no distinguishable change in the disulfide bridges for the single molecules could be detected. We assume that the vast majority of the interactions are covalent. However, in non-stressed materials, we observed that the dimers partially dissociate again. Non-covalent aggregates are lost during RPC separation and cannot be identified with the described mD-setup. To overcome this limitation, hydrophobic interaction chromatography will be tested in future follow-up studies. Further investigations are already underway, with indications of a number of different interaction variants and conformers formed per dimer variant, in line with previous reports.[37−40,44−48]

Overall, the mD-LC−MS/MS method facilitates the detailed characterization of a broad range of product variants. Furthermore, it provides essential information required for the validation of the traditional, less-specific, and lower-resolving, release testing methods, which are particularly challenged when applied to the size variant analysis of more complex emerging protein therapeutics such as co-formulations, bispecific antibodies, and other less-conventionally structured molecule types. The increased depth of information obtained by the online mD-LC−MS/MS method also supports attribute selection for LC−MS peptide mapping method development, especially critical when these are to be applied for release testing in multi-attribute monitoring strategies.

In summary, this study provides a demonstration of tools to identify and quantify aggregates in single and complex formulations. It indicates that co-aggregates may also have previously been present at low levels in other antibody co-formulations. Due to the lack of analytical approaches to detect heterogeneous and highly similar dimer forms, such species were elusive in the past; however, with the present workflow, detection and characterization can be realized.

ASSOCIATED CONTENT

Supporting Information

The Supporting Information is available free of charge at https://pubs.acs.org/doi/10.1021/acs.analchem.2c03099.

Size variant monitoring data by SE-HPLC, LC−MS peptide mapping data on structural alterations of the presented samples, RP-UHPLC data of the starting material, SE-HPLC and SEC-MS data of the enriched antibody dimer variants, a mD-LC−MS configuration scheme, and SE-HPLC, SEC-MS, and LC−MS data tables (PDF)

AUTHOR INFORMATION

Corresponding Author

Patrick Bulau − *Pharma Technical Development, F. Hoffmann-La Roche Ltd., 4070 Basel, Switzerland;* orcid.org/0000-0002-7121-2954; Email: patrick.bulau@roche.com

Authors

Felix Kuhne − *Pharma Technical Development, Roche Diagnostics GmbH, 82377 Penzberg, Germany; Institute of Hygiene, University of Münster, 48149 Münster, Germany*

Katrin Heinrich − *Pharma Technical Development, Roche Diagnostics GmbH, 82377 Penzberg, Germany*

Martin Winter − *Pharma Technical Development, Roche Diagnostics GmbH, 82377 Penzberg, Germany*

Jürgen Fichtl − *Pharma Technical Development, Roche Diagnostics GmbH, 82377 Penzberg, Germany*
Gabriel Hoffmann − *Pharma Technical Development, F. Hoffmann-La Roche Ltd., 4070 Basel, Switzerland*
Franziska Zähringer − *Pharma Technical Development, F. Hoffmann-La Roche Ltd., 4070 Basel, Switzerland*
Katharina Spitzauer − *Pharma Technical Development, Roche Diagnostics GmbH, 82377 Penzberg, Germany*
Monika Meier − *Pharma Technical Development, Roche Diagnostics GmbH, 82377 Penzberg, Germany*
Tarik A. Khan − *Pharma Technical Development, F. Hoffmann-La Roche Ltd., 4070 Basel, Switzerland*
Lea Bonnington − *Pharma Technical Development, Roche Diagnostics GmbH, 82377 Penzberg, Germany*
Katharina Wagner − *Pharma Technical Development, Roche Diagnostics GmbH, 82377 Penzberg, Germany*
Jan Olaf Stracke − *Pharma Technical Development, F. Hoffmann-La Roche Ltd., 4070 Basel, Switzerland*
Dietmar Reusch − *Pharma Technical Development, Roche Diagnostics GmbH, 82377 Penzberg, Germany*
Harald Wegele − *Pharma Technical Development, Roche Diagnostics GmbH, 82377 Penzberg, Germany*
Michael Mormann − *Institute of Hygiene, University of Münster, 48149 Münster, Germany*

Complete contact information is available at: https://pubs.acs.org/10.1021/acs.analchem.2c03099

Author Contributions

Conceptualization, F.K., J.F., and P.B.; data curation, F.K.; formal analysis, F.K.; investigation, F.K., K.H., M.W., K.S., and K.W.; methodology, F.K., K.H., G.H., F.Z., K.S., and M.M.; project administration, H.W., D.R., and P.B.; resources, H.W., J.O.S., and D.R.; supervision, M.M. and P.B.; visualization, F.K.; manuscript draft, F.K.; manuscript review and editing, F.K., T.A.K., L.B., M.M., and P.B.

Notes

The authors declare no competing financial interest.

■ ACKNOWLEDGMENTS

We are very grateful for lab support of and fruitful discussions with various members of the laboratories at Roche Diagnostics GmbH in Penzberg (Germany) and Roche Holding in Basel (Switzerland). Special gratitude goes to Dr. Linda Stemmle for her support with data analysis, to Genoveva Strobel for her support with SE-HPLC, to Dr. Anne Trefzer for her support with illustrations, and to Steffen Willmann for his support with downstream processing-related topics.

■ REFERENCES

(1) Kaplon, H.; Reichert, J. M. *mAbs* **2021**, *13*, 1860476.
(2) Kaplon, H.; Chenoweth, A.; Crescioli, S.; Reichert, J. M. *mAbs* **2022**, *14*, 2014296.
(3) Baselga, J.; Swain, S. M. *Clin. Breast Cancer* **2010**, *10*, 489−491.
(4) Rasmussen, S. K.; Næsted, H.; Müller, C.; Tolstrup, A. B.; Frandsen, T. P. *Arch. Biochem. Biophys.* **2012**, *526*, 139−145.
(5) Schmidt, C. *Nature* **2017**, *552*, S67−S69.
(6) Kaplon, H.; Reichert, J. M. *mAbs* **2018**, *10*, 183−203.
(7) Kim, J.; Kim, Y. J.; Cao, M.; De Mel, N. D.; Miller, M.; Bee, K.; Wang, J. S.; Wang, J.; Albarghouthi, X. *mAbs* **2020**, *12*, 1738691.
(8) Cao, M.; De Mel, N.; Shannon, A.; Prophet, M.; Wang, C.; Xu, W.; Niu, B.; Kim, J.; Albarghouthi, M.; Liu, D.; Meinke, E.; Lin, S.; Wang, X.; Wang, J. *mAbs* **2019**, *11*, 489−499.
(9) Sharma, V. K.; Misra, B.; McManus, K. T.; Avula, S.; Nellaiappan, K.; Caskey, M.; Horowitz, J.; Nussenzweig, M. C.; Seaman, M. S.; Javeri, I.; Dey, A. K. *Antibodies* **2020**, *9*, 36.
(10) Mueller, C.; Altenburger, U.; Mohl, S. *J. Pharm. Pharmacol.* **2018**, *70*, 666−674.
(11) Chauhan, V. M.; Zhang, H.; Dalby, P. A.; Aylott, J. W. *J. Controlled Release* **2020**, *327*, 397−405.
(12) Harris, R. J. *Dev. Biol.* **2005**, *122*, 117−127.
(13) Vlasak, J.; Ionescu, R. *Curr. Pharm. Biotechnol.* **2008**, *9*, 468−481.
(14) Beck, A.; Wagner-Rousset, E.; Ayoub, D.; Van Dorsselaer, A. V.; Sanglier-Cianférani, S. *Anal. Chem.* **2013**, *85*, 715−736.
(15) Schmid, I.; Bonnington, L.; Gerl, M.; Bomans, K.; Thaller, A. L.; Wagner, K.; Schlothauer, T.; Falkenstein, R.; Zimmermann, B.; Kopitz, J.; Hasmann, M.; Bauss, F.; Haberger, M.; Reusch, D.; Bulau, P. *Commun. Biol.* **2018**, *1*, 28.
(16) Haberger, M.; Bomans, K.; Diepold, K.; Hook, M.; Gassner, J.; Schlothauer, T.; Zwick, A.; Spick, C.; Kepert, J. F.; Hienz, B.; Wiedmann, M.; Beck, H.; Metzger, P.; Mølhøj, M.; Knoblich, C.; Grauschopf, U.; Reusch, D.; Bulau, P. *mAbs* **2014**, *6*, 327−339.
(17) Administration, US Food and Drug. *Guidance for Industry: Codevelopment of Two or More New Investigational Drugs for Use in Combination*; Center for Drug Evaluation and Research, US Food and Drug Administration: Rockville (MD), 2013.
(18) Rosenberg, A. S. *AAPS J.* **2006**, *8*, E501−E507.
(19) De Groot, A. S.; Scott, D. W. *Trends Immunol.* **2007**, *28*, 482−490.
(20) Lowe, D.; Dudgeon, K.; Rouet, R.; Schofield, P.; Jermutus, L.; Christ, D. *Adv. Protein Chem. Struct. Biol.* **2011**, *84*, 41−61.
(21) Haberger, M.; Leiss, M.; Heidenreich, A.-K.; Pester, O.; Hafenmair, G.; Hook, M.; Bonnington, L.; Wegele, H.; Haindl, M.; Reusch, D.; Bulau, P. *mAbs* **2015**, *8*, 331−339.
(22) Rosati, S.; Yang, Y.; Barendregt, A.; Heck, A. J. R. *Nat. Protoc.* **2014**, *9*, 967−976.
(23) Heck, A. J. R. *Nat. Methods* **2008**, *5*, 927−933.
(24) Michels, D. A.; Brady, L. J.; Guo, A.; Balland, A. *Anal. Chem.* **2007**, *79*, 5963−5971.
(25) Bansal, R.; Gupta, S.; Rathore, A. S. *Pharm. Res.* **2019**, *36*, 152.
(26) Pirok, B. W. J.; Stoll, D. R.; Schoenmakers, P. J. *Anal. Chem.* **2019**, *91*, 240−263.
(27) Oezipek, S.; Hoelterhoff, S.; Breuer, S.; Bell, C.; Bathke, A. *Anal. Chem.* **2022**, *94*, 8136−8145.
(28) Gstöttner, C.; Klemm, D.; Haberger, M.; Bathke, A.; Wegele, H.; Bell, C.; Kopf, R. *Anal. Chem.* **2018**, *90*, 2119−2125.
(29) Stoll, D.; Danforth, J.; Zhang, K.; Beck, A. *J. Chromatogr. B: Anal. Technol. Biomed. Life Sci.* **2016**, *1032*, 51−60.
(30) Reinders, L. M. H.; Klassen, M. D.; Teutenberg, T.; Jaeger, M.; Schmidt, T. C. *Anal. Bioanal. Chem.* **2021**, *413*, 7119−7128.
(31) Pot, S.; Gstöttner, C.; Heinrich, K.; Hoelterhoff, S.; Grunert, I.; Leiss, M.; Bathke, A.; Domínguez-Vega, E. *Anal. Chim. Acta* **2021**, *1184*, 339015.
(32) Camperi, J.; Goyon, A.; Guillarme, D.; Zhang, K.; Stella, C. *Analyst* **2021**, *146*, 747−769.
(33) Graf, T.; Heinrich, K.; Grunert, I.; Wegele, H.; Haberger, M.; Bulau, P.; Leiss, M. *J. Pharm. Biomed. Anal.* **2020**, *186*, 113251.
(34) Haberger, M.; Heidenreich, A.-K.; Hook, M.; Fichtl, J.; Lang, R.; Cymer, F.; Adibzadeh, M.; Kuhne, F.; Wegele, H.; Reusch, D.; Bonnington, L.; Bulau, P. *J. Am. Soc. Mass Spectrom.* **2021**, *32*, 2062−2071.
(35) Kuhne, F.; Bonnington, L.; Malik, S.; Thomann, M.; Avenal, C.; Wegele, F.; Reusch, H.; Mormann, D.; Bulau, M.; Cymer, P. *Antibodies* **2019**, *8*, 49.
(36) Diepold, K.; Bomans, K.; Wiedmann, M.; Zimmermann, B.; Petzold, A.; Schlothauer, T.; Mueller, R.; Moritz, B.; Stracke, J. O.; Mølhøj, M.; Reusch, D.; Bulau, P. *PLoS One* **2012**, *7*, No. e30295.
(37) Liu, M.; Zhang, Z.; Cheetham, J.; Ren, D.; Zhou, Z. S. *Anal. Chem.* **2014**, *86*, 4940−4948.
(38) Mason, B. D.; Schöneich, C.; Kerwin, B. A. *Mol. Pharmaceutics* **2012**, *9*, 774−790.

(39) Mozziconacci, O.; Kerwin, B. A.; Schöneich, C. *Chem. Res. Toxicol.* **2010**, *23*, 1310−1312.
(40) Paul, R.; Graff-Meyer, A.; Stahlberg, H.; Lauer, M. E.; Rufer, A. C.; Beck, H.; Briguet, A.; Schnaible, V.; Buckel, T.; Boeckle, S. *Pharm. Res.* **2012**, *29*, 2047−2059.
(41) Kerwin, B. A.; Remmele, R. L. *J. Pharm. Sci.* **2007**, *96*, 1468−1479.
(42) Edelman, G. M.; Cunningham, B. A.; Gall, W. E.; Gottlieb, P. D.; Rutishauser, U.; Waxdal, M. J. *Proc. Natl. Acad. Sci. U.S.A.* **1969**, *63*, 78−85.
(43) Jia, M.; Mozziconacci, O.; Abend, A.; Wuelfing, W. P.; Pennington, J. *Int. J. Mass Spectrom.* **2022**, *471*, 116725.
(44) Bommana, R.; Chai, Q.; Schöneich, C.; Weiss, W. F.; Majumdar, R. *J. Pharm. Sci.* **2018**, *107*, 1498−1511.
(45) Bane, J.; Mozziconacci, O.; Yi, L.; Wang, Y. J.; Sreedhara, A.; Schöneich, C. *Pharm. Res.* **2017**, *34*, 229−242.
(46) Haywood, J.; Mozziconacci, O.; Allegre, K. M.; Kerwin, B. A.; Schöneich, C. *Mol. Pharmaceutics* **2013**, *10*, 1146−1150.
(47) Amano, M.; Kobayashi, N.; Yabuta, M.; Uchiyama, S.; Fukui, K. *Anal. Chem.* **2014**, *86*, 7536−7543.
(48) Plath, F.; Ringler, P.; Graff-Meyer, A.; Stahlberg, H.; Lauer, M. E.; Rufer, A. C.; Graewert, M. A.; Svergun, D.; Gellermann, G.; Finkler, C.; Stracke, J. O.; Koulov, A.; Schnaible, V. *mAbs* **2016**, *8*, 928−940.

https://doi.org/10.1021/acs.analchem.2c03099
Anal. Chem. 2023, 95, 2203−2212